International Journal of Computational Methods
Vol. 12, No. 4 (2015) 1540005 (24 pages)

DOI: 10.1142/S0219876215400058

Prediction of Solid Recirculation Rate and Solid Volume Fraction in an Internally Circulating Fluidized Bed

Ravi Gujjula*,†,‡ and Narasimha Mangadoddy*,§

*Department of Chemical Engineering
Indian Institute of Technology Hyderabad
Ordnance Factory Estate, Medak
Telangana, 502205, India

†Department of Petroleum Engineering
K L University, Vaddeswaram
Vijayawada, Andhraprades 522 502, India
‡ravigujjula@gmail.com
§narasimha@iith.ac.in

Received 20 September 2014
Revised 11 December 2014
Accepted 27 December 2014
Published 1 April 2015

This paper presents a numerical study of gas and solid flow in an internally circulating fluidized bed (ICFB). Two-fluid Eulerian model with kinetic theory of granular flow option for solid phase stress closure and various drag laws were used to predict the hydrodynamic behavior of ICFB. 2D and 3D geometries were used to run the simulations. The 2D simulation results by various drag laws show that the Arastoopour and Gibilaro drag models able to predict the fluidization dynamics in terms of flow patterns, void fractions and axial velocity fields close to the experimental data. The effect of superficial gas velocity, presence of draft tube on solid hold-up distribution, solid circulation pattern, and variations in gas bypassing fraction for the 3D ICFB are investigated. The mechanism governing the solid circulation and solids concentration in an ICFB has been explained based on gas and solid dynamics obtained from the simulations. Predicted total granular temperature distributions in the draft tube and annular zones qualitatively agree with experimental data. The total granular temperature tends to increase with increasing solids concentration in the dilute region ($\varepsilon < 0.1$) and decreases with an increase of solids concentration in the dense region ($\varepsilon > 0.1$). In the dense zone, the decreasing trend in the granular temperature is mainly due to the reduction of the mean free path of the solid particles.

Keywords: Internally circulating fluidized bed; two fluid model; solid recirculation rate; hydrodynamics.

‡Corresponding author.

Nomenclature

C_D	:	Drag coefficient
d_p	:	Particle diameter (m)
e_s	:	Coefficient of restitution
g	:	Acceleration due to gravity (m/s^2)
$g_o(\varepsilon_s)$	:	Radial distribution function
G_s	:	Solid recirculation rate (kg/m^{2}s)
I	:	Unit tensor
k	:	Diffusion coefficient of granular temperature (kg/ms)
P	:	Pressure (N/m^2)
P_s	:	Granular pressure (N/m^2)
R	:	Radius of ICFB (m)
r	:	Draft tube radius (m)
Re_p	:	Particle Reynolds number
U_a	:	Superficial velocity in the annulus (m/s)
U_d	:	Superficial velocity in the draft tube (m/s)
V_{rs}	:	Terminal velocity (m/s)
$v_s^{'}$	:	Ensemble averaged magnitude of the randomly fluctuating velocity of the solid particles (m/s)
v_s	:	Solid velocity (m/s)
v_g	:	Air velocity (m/s)

Greek Symbols

β	:	Inter-phase momentum transfer coefficient (kg/m^{3}s)
λ_s	:	Granular bulk viscosity (kg/ms)
μ_s	:	Solid viscosity (kg/ms)
μ_g	:	Gas viscosity (kg/ms)
π	:	Irrational number
Θ_s	:	Granular temperature (m^2/s^2)
ε_g	:	Air volume fraction
ε_s	:	Solid volume fraction
γ	:	Collisional dissipation of energy (kg/m^{3}s)
ϕ_s	:	Transfer rate of kinetic energy (kg/m^{3}s)
ρ_g	:	Air density (kg/m^3)
ρ_s	:	Solid density (kg/m^3)
τ_g	:	Gas stress tensor (N/m^2)
τ_s	:	Solid stress tensor (N/m^2)

Subscripts

g	:	Gas phase
s	:	Solid phase

1. Introduction

Gas–solid fluidization by conventional circulating fluidized beds (CFB) are common in various industrial operations such as coal combustion and gasification, incineration of municipal solid waste, catalyst regeneration, thermal cracking and drying [Burugupalli (1988); Kim *et al.* (1997, 2000); Yang *et al.* (2008)]. They require very tall column as a solid raiser and accompanying additional external circulation of solids through a cyclone. In order to avoid external circulation accessories, a compact internally circulating fluidized bed (ICFB) was developed, which is a modified spouted fluidized bed with a draft tube inside the column to avoid problem of gas bypassing. An ICFB is having a centrally located draft tube that divides the bed into two or more sections and thus promotes solid circulation within a single vessel [Burugupalli (1988); Chatterjee (1970); Kim *et al.* (1997); Yang and Keairns (1978)]. This ICFB reactor has many advantages such as its compact size and the annular section act as heat sink because riser is located inside the vessel [Jeon and Kim (2010); Milne *et al.* (1992)]. The ICFB reduces the height of conventional CFB riser and construction cost, solves the problems of CFB, makes highly efficient and low pollution combustion for a wide range of fuels. In ICFB, the draft tube (or riser) was fixed directly to the gas distributor of the riser section [Kim *et al.* (2002)].

In recent years due to advances in high performance computers and numerical algorithms, the computational fluid dynamics (CFD) technique has become a fundamental element of research in simulating gas–solid multiphase flow systems [Mujumdar and Wu (2008)]. Thus many researchers have put considerable effort in validating the CFD models in order to achieve fundamental and accurate model for these systems. One of the difficulties to validate CFD models using experimental measurements is the computational effort needed to perform three-dimensional (3D) simulations of dynamic behavior of industrial scale fluidized beds.

In the past, a number of computational studies on fluidization indicated that the drag force between particle and fluid plays an important role in predicting the flow structure of CFBs [Beetstra *et al.* (2007); Helland *et al.* (2007); McKeen and Pugsley (2003); Yang *et al.* (2003); Zimmermann and Taghipour (2005)]. Several specific drag models have been developed to calculate the inter-phase momentum exchange in fluidized beds [Gidaspow (1994); Syamlal and O'Brien (1989); Wen and Yu (1966)]. Many researchers have simulated the circulating fluidized bed of fluid catalytic cracking (FCC) particles using the classical drag models [Benyahia *et al.* (2000); Chan *et al.* (2005); Neri and Gidaspow (2000); Zheng *et al.* (2001)]. However, few successful simulations were reported on dense fluidization of Geldart A particles. The CFD modeling of a bubbling FCC fluidized-bed reactor by Zimmermann and Taghipour [2005] showed that the Syamlal–O'Brien and Gidaspow drag models overestimated the momentum exchange between the gas and the solid phase and the bed expansion in comparison to the experimental data. The effect of various drag models on hydrodynamics behavior of gas–solid fluidized beds was also compared by VanWachem *et al.* [2001]. They found that the expression suggested by

Syamlal–O'Brien [1989] model underpredicts the pressure drop, bed expansion and bubble diameter compared to the experimental data. McKeen and Pugsley [2003] simulated a freely bubbling bed of FCC particles with a two-fluid model (TFM). It was found that the generally poor simulation results for Geldart A particles could be attributed to the existence of significant cohesive inter-particle forces. Hosseini *et al.* [2009] simulated the bubbling fluidized bed of FCC particles at high superficial gas velocities and demonstrated the sensitivity of their system to the model's parameters such as drag function, restitution coefficient, and maximum solid packing limits. They have observed significant errors between the predicted bed expansion ratios in comparison to the experimental data. Using the Gibilaro's drag model [1985] with a suitable scale factor, it was found more reasonable hydrodynamics results. In addition to the gravitational and the drag forces, several researchers have also shown that the frictional stresses play an important role in the modeling of a fluidization process [Abu-Zaid and Ahmadi (1990); Huilin *et al.* (2004); Passalacqua and Marmo (2009); Patil and van Sint Annaland (2005); Patil *et al.* (2005); Reuge *et al.* (2008); Shuyan *et al.* (2009); VanWachem *et al.* (2001)]. Abu-Zaid and Ahmadi [1990] developed a simple kinetic model for flow of nearly elastic granular materials in the grain-inertia regime. They showed that frictional losses have the same effects as energy dissipation due to the inelasticity of granular particles. Reuge *et al.* [2008] and Hosseini *et al.* [2009] found excellent simulation results using the frictional model of Srivastava and Sundaresan [2003], when compared with the frictional models of Syamlal *et al.* [1993] and Johnson and Jackson [1987] for bubbling fluidized bed and spouted bed with a nonporous draft tube, respectively.

Understanding of the hydrodynamics of ICFB is still far away from its maturity when compared to CFBs. However, only few researchers have attempted to study the flow patterns in the ICFB in which most of the studies are limited two dimensional. In the early 2000s numerical model established based on the mass and momentum conservation equations to describe the complex hydrodynamics of ICFB reactor [Marschall and Mleczko (1999)]. Zhao *et al.* [2008] studied the particle motion in a two-dimensional thin slot-rectangular spouted bed with draft plates using particle image velocimetry (PIV). CFD simulations for grains of 0.22, 2.0, 3.7 and 1.0 mm diameter with the ICFB, confirmed that fluctuations are caused by particle clusters originating at the bottom of the column [Szafran and Kmiec (2007)]. Solid particles were seen to cross into the jet, cover the column inlet, and be transported periodically through the draft tube, which is contrary to the findings of Zhao *et al.* [2008]. The fluctuating solids inflow produces slugs and explains variations in fountain height and porosity. Modified and extended scaling relationships were proposed by Shirvanian and Calo [2004] for conical-based rectangular spouted vessels with draft tube. The effect of superficial gas velocity, position of the draft tube and type of sparging action on the ICFB solid hold-up and the solid circulation patterns studied through physical experiments and 2D CFD simulations by Ahuja and Patwardhan [2008]. Hosseini *et al.* [2010] predicted the hydrodynamics

of ICFB reactor with 2D CFD integrating kinetic theory of granular flow (KTGF) to achieve accurate simulation of the gas–solid fluidized beds. They demonstrated with that the adopted CFD model can capture the key features of an ICFB system, fast fluidization in the reaction chamber, bubbling fluidization in the heat exchanger chamber and solid circulation between the chambers [Feng *et al.* (2012)]. Although 2D pseudo simulations predict the hydrodynamic parameters reasonably correct, but the accurate prediction of solids volume fraction distributions and its associated fluctuate velocity components via granular temperature equations is only possible with 3D simulations. Very little literature exists on the granular temperature profiles of ICFB's, in which downward moving annulus bed of solids significantly influence the draft tube riser solids dynamics unlike risers in the CFBs. 3D simulations of ICFB are virtually nonexist. Usually fast fluidized beds are always dynamic and turbulent in nature, to account this turbulence 2D simulation is not able to predict the dynamics correctly due to less space availability in 2D.

The work reported in this paper is aimed to develop a CFD-model for the hydrodynamic study of 2D and 3D ICFB reactors. The two-fluid flow CFD model along with the k–ε turbulence model and solid stress closer from KTGF is used for simulating the gas–solid flow pattern. With the help of these simulations the instantaneous and the time-averaged pressure drop profiles and the solid volume fractions within the draft tube and the annulus section of ICFB are calculated. Further, the flow fields, i.e., volume fractions and velocity distributions are predicted for different size particles in the range of 86–250 μm. A series of 2D-ICFB CFD simulations were also run to validate the CFD model predictions against the Ahuja and Patwardhan [2008] experimental data. This CFD methodology also adopted to investigate gas–solid flow dynamics for the large scale 3D ICFB geometry extensively. An attempt to compute the granular temperature for 3D ICFB and its validation against literature experimental data is made.

2. Methodology

2.1. *Eulerian–Eulerian model equations for gas–solid flow with KTGF*

In the present study, it is proposed to solve the governing equations of mass, momentum and granular energy for both the gas and solids phase by means of a TFM approach incorporating the KTGF available in the commercial software package ANSYS's FLUENT^{TM}. To solve the set of equations, closures laws are required. The closure relations based on the KTGF are utilized. The details of closure models, physical properties and simulation parameters used in this study are described in the following sections. The partial differential TFM equations for explaining particle and fluid flows in the fluidized bed [Patankar (1980)] were adopted for the 2D

and 3D ICFB. The continuity equation in the absence of mass transfer between the phases is given for each phase as follows

Continuity equations

$$\frac{\partial}{\partial t}(\varepsilon_g \rho_g) + \nabla \cdot (\varepsilon_g \rho_g v_g) = 0, \tag{1}$$

$$\frac{\partial}{\partial t}(\varepsilon_s \rho_s) + \nabla \cdot (\varepsilon_s \rho_s v_s) = 0, \tag{2}$$

$$\varepsilon_g + \varepsilon_s = 1. \tag{3}$$

Momentum conservation equations

$$\frac{\partial}{\partial t}(\varepsilon_g \rho_g \upsilon_g) + \nabla \cdot (\varepsilon_g \rho_g \upsilon_g \upsilon_g) = \nabla \cdot \tau_g + \varepsilon_g \rho_g g - \varepsilon_g \nabla P + \beta(\upsilon_g - \upsilon_s), \tag{4}$$

$$\frac{\partial}{\partial t}(\varepsilon_s \rho_s \upsilon_s) + \nabla \cdot (\varepsilon_s \rho_s \upsilon_s \upsilon_s) = \nabla \cdot \tau_s + \varepsilon_s \rho_s g - \nabla P_s - \varepsilon_s \nabla P + \beta(\upsilon_g - \upsilon_s). \tag{5}$$

2.2. *Solid phase stress model formulations*

To close the solid phase momentum transport equations, the solid phase stresses should be described. The kinetic theory concept can be used for calculating the effective stresses of the solid phase resulting from direct collision and particle streaming. These concepts are used when the granular motion is dominated by collision interactions. In the modeling of granular flow, particles are modeled in analogy to gas molecules; hence the granular temperature may be defined in analogy to the temperature of gas. In this, a relation exists between molecules random motion and temperature. The granular temperature is a measurement of the random fluctuations of the molecules in any substance. Random fluctuations are at a micro level in the molecules. This theory is extended to the macro scale where the molecules are substituted with particles. This approach is referred as the KTGF and as described by Lun *et al.* [1984]. The solid pressure is composed of a kinetic term and a second term due to particle collisions as follows [Lun *et al.* (1984)]. KTGF has become a very key tool for modeling gas–particle fluidized bed. Various studies on the hydrodynamics of gas–solid fluidized bed incorporating the KTGF have shown this theory as the promising approach. These studies were also conducted by various researchers [Sinclair and Jackson (1989); Benyahia *et al.* (2000)]. The kinetic energy of granular mean flow first degrades into the kinetic energy of random particle fluctuations, and then dissipates as heat because of inelastic collisions. Analogous to the thermodynamic temperature for gases, the granular temperature can be introduced as a measure of the particle velocity fluctuation. The granular temperature conservation equation is mentioned below. Granular temperature is defined as

$$\Theta_s = \frac{1}{3}\langle \overline{\upsilon_s' \upsilon_s'} \rangle. \tag{6}$$

Conservation of the kinetic energy of the moving particles is described based on granular temperature Θ_s as

$$\frac{3}{2}\left[\frac{\partial}{\partial t}(\varepsilon_s\rho_s\Theta_s)+\nabla\cdot(\varepsilon_s\rho_s\upsilon_s\Theta_s\right]=\tau_s:\nabla\upsilon_s-\nabla\cdot(k\Theta_s\nabla\Theta_s)-\gamma_{\Theta s}-\phi_s. \quad (7)$$

In the above equation, υ_s represents the ensemble averaged magnitude of solid phase velocity, υ_s' represents the magnitude of fluctuating velocity of the solid particles. τ_s is solid stress tensor, $k_{\Theta s}\nabla\Theta_s$ is flux of fluctuating energy represents conduction due to the gradient of granular temperature represents the diffusion of the energy, $\gamma_{\Theta s}$ is collisional dissipation of energy due to inelastic particle collisions. This term is represented by the expression derived by Lun *et al.* [1984], ϕ_s is the transfer rate of kinetic energy between fluid–solid phases. $k_{\Theta s}$, $\gamma_{\Theta s}$ and ϕ_s equations are mentioned in Eqs. (8)–(10), respectively.

$$k_{\Theta s}=\frac{150d_p\rho_s\sqrt{\Theta_s\pi}}{384(1+e)g_o(\varepsilon_s)}\left[1+\frac{6}{5}(1+e)\varepsilon_g g_o(\varepsilon_s)\right]^2+2d_p\rho_s\varepsilon_s^2(1+e)g_o(\varepsilon_s)\sqrt{\frac{\Theta_s}{\pi}}, \quad (8)$$

$$\gamma_{\Theta s}=\frac{12(1-e_s^2)g_{os}}{d_s\sqrt{\pi}}\rho_s\varepsilon_s^2\Theta_s^{3/2}, \quad (9)$$

$$\phi_s=-3\beta\Theta_s. \quad (10)$$

2.3. *Solids pressure*

The solid particles pressure is calculated independently and is used for the pressure gradient term ∇P_s in the solid granular phase momentum equation (5). The solid pressure is composed of a kinetic term and a second term due to particle collisions as follows

$$P_s=\varepsilon_s\rho_s\Theta_s+2\rho_s(1+e_s)\varepsilon_s^2g_o(\varepsilon_s)\Theta_s, \quad (11)$$

$$\tau_s=\varepsilon_s\mu_s(\nabla\upsilon_s+(\nabla\upsilon_s)^T)+\varepsilon_s\left(\lambda_s-\frac{2}{3}\mu_s\right)(\nabla\cdot\upsilon_s)\cdot I, \quad (12)$$

$$\tau_g=\varepsilon_g\mu_g(\nabla\upsilon_g+(\nabla\upsilon_g)^T)-\frac{2}{3}\varepsilon_g\mu_g(\nabla\cdot\upsilon_g)\cdot I, \quad (13)$$

where Θ_s is the granular temperature, $g_o(\varepsilon_s)$ is the radial distribution function which depends on solids volume fraction (ε_s), and e_s is the coefficient of restitution for particle collisions. The coefficient $e_s=0.9$ is used in the simulations. The granular temperature Θ_s is proportional to the kinetic energy of the fluctuating particle motion. τ_s solid stress tensor can be expressed in Eq. (12) and (13) for gas–solid system respectively.

Where μ_s and λ_s are the shear bulk and granular bulk viscosities in the solid phase, d_p is the particle diameter and π is the irrational number. The following model is adopted from KTGF by Lun *et al.* [1984] granular Kinetic theory

The following sub models used to account solid shear viscosity in the solid granular phase

Solids bulk viscosity, [Lun *et al.* (1984)]

$$\lambda_s = \frac{4}{3}\varepsilon_s\rho_s d_p g_0(\varepsilon_s)(1+e_s)\sqrt{\frac{\Theta_s}{\pi}}, \tag{14}$$

Granular viscosity, [Syamlal *et al.* (1993)]

$$\mu_{s,\text{kin}} = \frac{\varepsilon_s\rho_s d_s\sqrt{\Theta_s}\pi}{6(3-e_s)}\left[1+\frac{2}{5}(1+e_s)(3e_s-1)\varepsilon_s g_0(\varepsilon_s)\right], \tag{15}$$

Frictional viscosity, [Schaeffer (1987)]

$$\mu_{s,\text{fr}} = \frac{P_s \text{Sin}\phi}{2\sqrt{I_2 D}}, \tag{16}$$

Collisional viscosity

$$\mu_{s,\text{col}} = \frac{4}{5}\varepsilon_s\rho_s d_p g_0(\varepsilon_s)(1+e_s)\sqrt{\frac{\Theta_s}{\pi}}. \tag{17}$$

The radial distribution function, $g_0(\varepsilon_s)$, that governs the transition from the "compressible" condition with $\varepsilon_s < \varepsilon_{s,\max}$, where the spacing between the solid particles can continue to decrease, to the "incompressible" condition with $\varepsilon_s > \varepsilon_{s,\max}$ where no further decrease in the spacing can occur. The radial distribution function can be seen as a measure for the probability of inter-particle contact and estimated by Eq. (18). The radial distribution function $g_0(\varepsilon_s)$ is a correction factor that modifies the probability of collision close to packing as suggested by Sinclair and Jackson [1983]. $\varepsilon_{s,\max}$ is the maximum solids volume fraction for the packing limit.

$$g_o(\varepsilon_s) = \left(1-\left(\frac{\varepsilon_s}{\varepsilon_{s,\max}}\right)^{\frac{1}{3}}\right)^{-1}. \tag{18}$$

2.4. *Drag models*

The mathematical formulations of the four drag models that have been used in this work are shown below.

Gidaspow's drag model [1994]

$$\beta_{\text{Wen-Yu}} = \frac{3C_D\varepsilon_s\varepsilon_g\rho_g|v_g-v_s|}{4d_p}\varepsilon_g^{-2.65}, \quad \varepsilon_g \geq 0.8, \tag{19}$$

$$\beta_{\text{Ergun}} = 150\frac{\varepsilon_s^2\mu_g}{\varepsilon_g d_p^2} + 1.75\frac{\varepsilon_s\mu_g|v_g-v_s|}{d_p}, \quad \varepsilon_g < 0.8, \tag{20}$$

$$C_D = \begin{cases} \dfrac{24}{\text{Re}_p}[1+0.15(\text{Re}_p)^{0.687}], & \text{Re}_p < 1000, \\ 0.44, & \text{Re}_p > 1000, \end{cases} \tag{21}$$

$$\mathrm{Re}_p = \frac{\varepsilon_g \rho_g d_p |\upsilon_g - \upsilon_s|}{\mu_g}, \quad \text{Particle Reynolds number.} \tag{22}$$

Arastoopour's drag model [1990]

$$\beta_{\mathrm{gs}} = \left(\frac{17.3}{\mathrm{Re}_p} + 0.336\right) \frac{\rho_g |\upsilon_g - \upsilon_s|}{d_p} (1 - \varepsilon_g) \varepsilon_g^{-2.8}. \tag{23}$$

Syamlal–O'Brien [1989]

$$\beta_{\mathrm{gs}} = \frac{3}{4} \frac{\varepsilon_g \varepsilon_s \rho_g}{\nu_{rs}^2 d_p} C_D \left(\frac{\mathrm{Re}_p}{\nu_{rs}}\right) |\upsilon_g - \upsilon_s|, \tag{24}$$

$$C_D = \left(0.63 + \frac{4.8}{\sqrt{\mathrm{Re}_p / \nu_{\mathrm{rs}}}}\right)^2, \tag{25}$$

$$\mathrm{Re}_p = \frac{\rho_g d_p |\upsilon_g - \upsilon_s|}{\mu_g}, \tag{26}$$

$$\nu_{\mathrm{rs}} = 0.5[A - 0.06\mathrm{Re}_p + \sqrt{(0.06\mathrm{Re}_p)^2 + 0.12\mathrm{Re}_p(2B - A) + A^2}], \tag{27}$$

$$A = \varepsilon_g^{4.14}, \quad B = \begin{cases} 0.8\varepsilon_g^{1.28} & \text{for } \varepsilon_g \le 0.85, \\ \varepsilon_g^{2.65} & \text{for } \varepsilon_g \ge 0.85. \end{cases} \tag{28}$$

Gibilaro's drag model [1985]

$$\beta_{\mathrm{gs}} = \left(\frac{17.3}{\mathrm{Re}_p} + 0.336\right) \frac{\rho_g |\upsilon_g - \upsilon_s|}{d_p} (1 - \varepsilon_g) \varepsilon_g^{-1.80}, \tag{29}$$

$$\mathrm{Re}_p = \frac{\varepsilon_g \rho_g d_p |\upsilon_g - \upsilon_s|}{\mu_g}. \tag{30}$$

Figure 1 shows the relationship between the fluid–solid phase exchange coefficient, which is estimated for the available drag models in the literature as a function

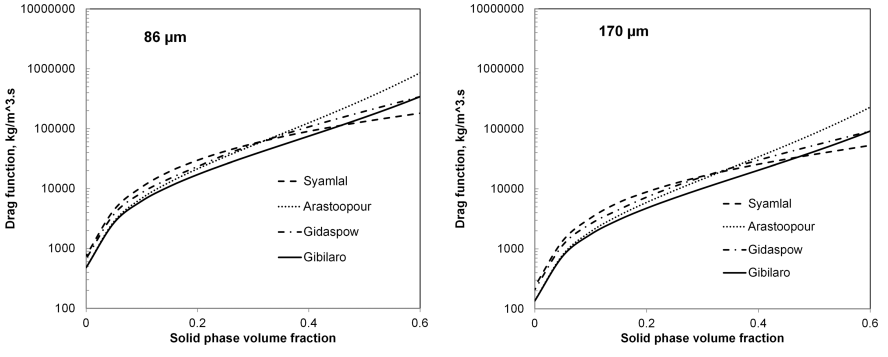

(a) (b)

Fig. 1. Comparison of different drag models for (a) 86 μm particles, (b) 170 μm particles, (c) 250 μm particles and (d) 853 μm particles at a slip velocity of 1.04 m/s.

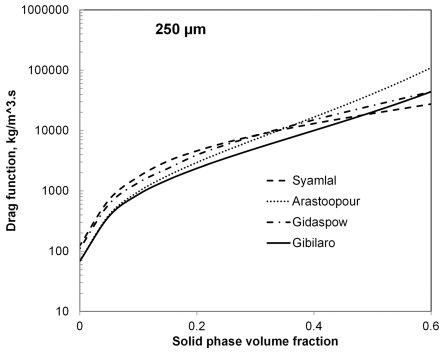

(c)

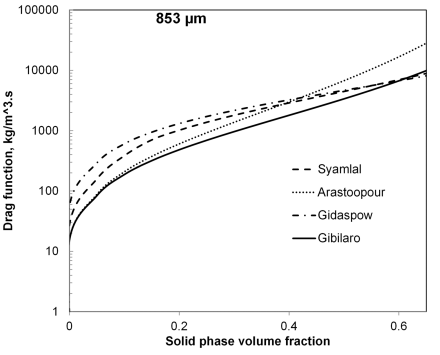

(d)

Fig. 1. (*Continued*)

of solids volume fraction. For various drag models at fixed slip velocity of 1.04 m/s and for the 86, 170 and 250 μm particles used in the present study calculations of Fig. 1. It is evident that the Arastoopour and Gibilaro drag models predict larger values of gas–solids exchange coefficient at higher values of solids concentration compared to Syamlal–O'Brien and Gidaspow drag models. This means that the Arastoopour and Gibilaro drag models-based predictions significantly differ near the walls and drag coefficient will have the greatest influence on the model. Figure 1(d) shows the quantitative comparison of various drag models at fixed slip velocity of 1.04 m/s and for the 853 μm particles used in the present study as part of validation. There will be a slight difference between drag coefficients at both low and very high solid concentration zones for the coarsest particles, i.e., 853 μm.

3. Simulation Strategy and Conditions

In this paper, simulations were run with two different ICFB geometries having an internal draft tube. First geometry, 2D ICFB is considered from Ahuja and Patwardhan, [2008] work, used for validation of the CFD model. The second geometry, 3D ICFB of IITH's, with 30 cm diameter fluidization rig was used for parametric analysis. Ahuja and Patwardhan, [2008] experimented solid-gas flow patterns in ICFB with a small geometry (column 0.186 m × 1.2 m with a draft tube of 0.10 m × 0.158 m) by considering a particular case partial sparging with a draft tube (see Fig. 2(a)), 2D simulations were performed using Eulerian–Eulerian TFM along with no-slip boundary conditions for both phases at the ICFB walls. Solids volume fraction was defined as 0.62 with a maximum packing limit of 0.65. Simulation was initiated with uniform inlet superficial gas velocity of 1.041 m/s.

In this work, the 3D geometry of ICFB (0.3 m × 3.0 m and draft tube 0.1 m × 0.9 m) height draft tube was used shown in Fig. 2(b). Grid consists of total 46,536 nodes and two cell zones. The initial bed height of 0.86 m was considered and the initial solid volume fraction was defined as 0.62 with a maximum packing of 0.65. Simulation was initiated with uniform inlet superficial gas velocity to the draft tube

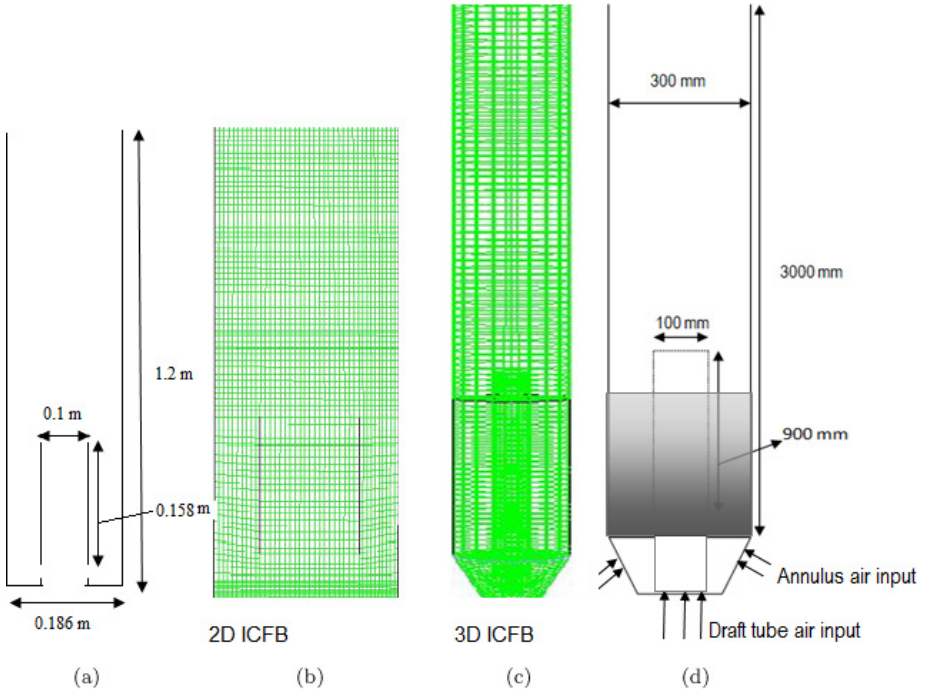

Fig. 2. Schematic diagrams of 2D ICFB: (a) Geometry and (b) grid and 3D ICFB: (a) Grid and (b) geometry.

was set as 0.8, 1.25, 1.5 and 1.75 m/s with a constant uniform gas velocity of 0.2 m/s as an input to the annular section.

Simulations were run using ANSYS's FLUENT 12.1.3 software with a standard k–ε model and Eulerain–Eulerian methods. Phase Coupled Semi Implicit Method for Pressure Linked Equations (PC-SIMPLE), which is an extension of Semi Implicit Method for Pressure Linked Equations (SIMPLE) algorithm to multiphase flows, was applied for pressure–velocity coupling. In this algorithm, the coupling terms are treated implicitly.

The pressure velocity coupling which was based on total volume continuity and the effect of the interfacial coupling terms are completely incorporated into the pressure correction equation. QUICK scheme is used for discretizing the governing equations. A fixed time stepping of 0.001 s was used to advance the solution time. Table 1 shows a set of conditions and parameters used in simulations.

4. Results and Discussion

4.1. *Grid independence check*

Grid independence check was initially performed for 2D 186 mm ICFB simulations. Based on assessment of analytical gas–solid exchange coefficient described in Fig. 1,

Table 1. Simulation and model parameter.

Parameter description	Value
Particle density	2500 (kg/m^3)
Air density	1.225 (kg/m^3)
Mean particle diameter	86,170 and 250 (μm)
Initial solid packing	0.62
Superficial air velocity	0.8, 1.0, 1.25, 1.5, 1.75 (m/s)
Fluidized bed column dimension	0.3 (m) × 3.0 (m)
Static bed height	0.8 (m)
Restitution coefficient	0.95
Boundary Condition	Outlet-pressure, walls-No slip

Arastoopour drag-based CFD model simulations are run to test the grid independence check. Four different mesh sizes comprising 5000, 10,000, 30,000 and 70,000 nodes were used for this study. The simulated 2D ICFB results in terms of solids hold-up by various grids are shown in Figs. 3 and 4. It is observed that simulations having grid size 30k and above are predicting the solid volume fractions close to the Ahuja's experimental data. Grid consisting 5 and 10k are underpredicting the solid volume fractions across the radial position. Hence grid size of 30k nodes is selected as an optimum grid size for all 2D ICFB simulations.

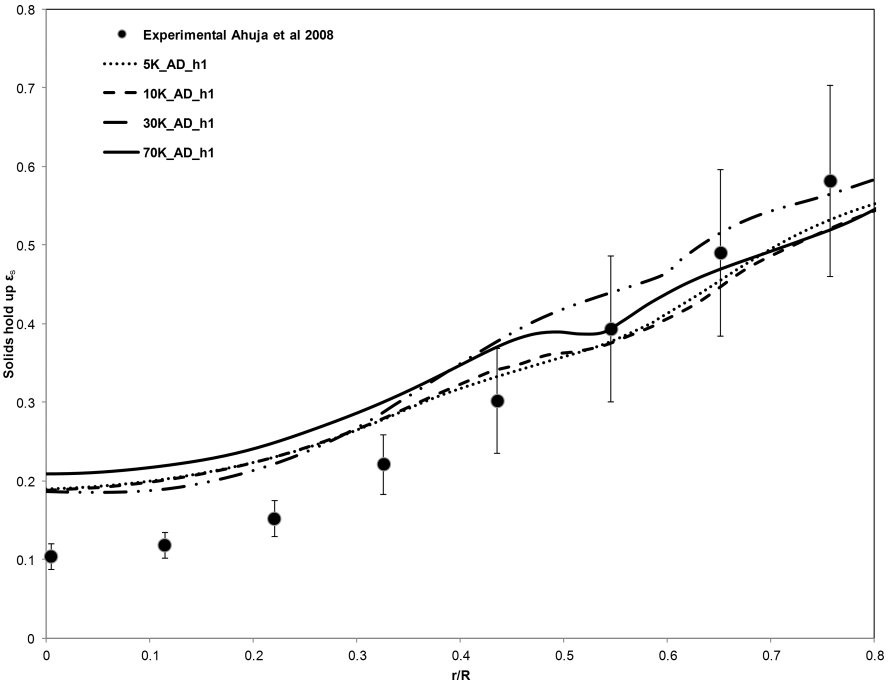

Fig. 3. Solids hold-up profiles for partial sparging with a draft tube comparison of different grid sizes with Arastoopour drag model.

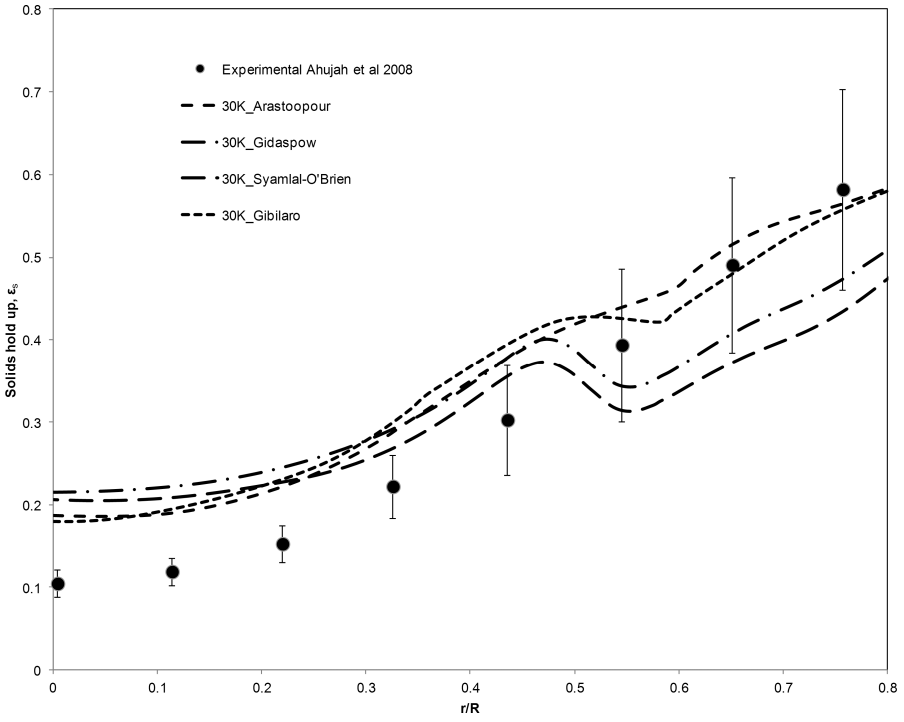

Fig. 4. Solids hold-up profiles for partial sparging with a draft tube: Comparison of different drag models of 853 μm particles with 30k grid.

4.2. *2D CFD predictions for* 186 mm *ICFB and validation*

In the current study, a number of momentum interface drag forces namely Gidaspow, Syamlal–O'Brien, Gibilaro and Arastoopour drag models are tested and compared with the Ahuja and Patwardhan [2008]'s experimental data to identify the suitable drag model for modeling the turbulent fluidization of gas–solid particles. In the present work, consider the case of Ahuja and Patwardhan [2008] experiments having partial and complete sparging for 2D-ICFB CFD runs operating at a 2.24 m/s superficial velocity.

The effect of different drag models on local solid hold-up at a superficial gas velocity of 2.24 m/s, the restitution coefficient 0.95, solid maximum packing of 0.65 at a height of $h = 0.0465$ m are shown in Fig. 4. It is observed that the Gidaspow and Syamlal–O'Brien drag models show the significantly deviating volume fraction values from experimental values. Arastoopour and Gibilaro drag models are predicting the solid volume fraction values much close to the experimental data. As observed from Fig. 1, the Gidaspow and Syamlal–O'Brien drag models underpredict the gas–solids interphase exchange coefficient at higher solids concentrations compared to the Arastoopour drag model. The drag forces accounted by Gibilaro [1990] and Arastoopour *et al.* [1990] are reasonably accurate and thus close predictions to

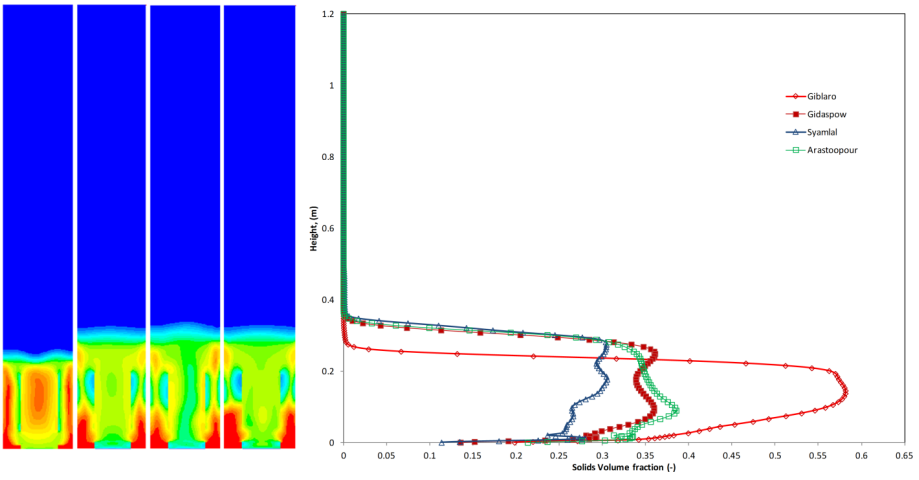

Fig. 5. The simulated solid volume fraction contours for various drag models for partially sparging with a draft tube ($Uo = 1.0425$ m/s). (a) Gibilaro drag model, (b) Gidaspow drag model, (c) Syamlal–O'Brien drag model and (d) Arastoopour drag model.

experimental data were observed. The simulated results of the 2D ICFB are presented in Figs. 4 and 5 in terms of solid volume fraction redial profiles and contours. In Figs. 5(a) and 5(b), comparison between various drag model predictions are made based on mean solid volume fraction contours. These contours data is analyzed in terms of expanded bed height and shape of fluidization pattern in Fig. 5(b). The Gibilaro and Arastoopour drag model prediction represents the low bed expansion comparatively with other drag model predictions. The CFD models of Gidaspow and Syamlal–O'Brien drag models predict lean solids zone just above the gas distributor as seen in Fig. 5, whereas Arastoopour and Gibilaro drag models predicts dense zone at the bottom of draft tube which is just above the gas distributor.

4.3. 300 mm *ICFB 3D simulations*

4.3.1. *Pressure drop*

The mean ΔP value is plotted to compare pressure difference at different axial locations in 3D ICFB column as shown in Figs. 6(a) and 6(b). The pressure drop in the draft tube passed through minima with an increase of gas superficial velocity. In the low velocity region the pressure drop decreased steadily. After minimum fluidization stage, once transport of solids movement is upward then the pressure drop decreases with an increase of superficial velocity due to the lean solids hold-up in the draft tube. The pressure drop at different heights of draft tube is following a decline trend with superficial gas velocity except at location of 0.25 m, which is just above the air distributor. At a height of 0.25 m location, part of draft tube gas gets into bypassing towards annular region and the ΔP seems unchanged at this gap area.

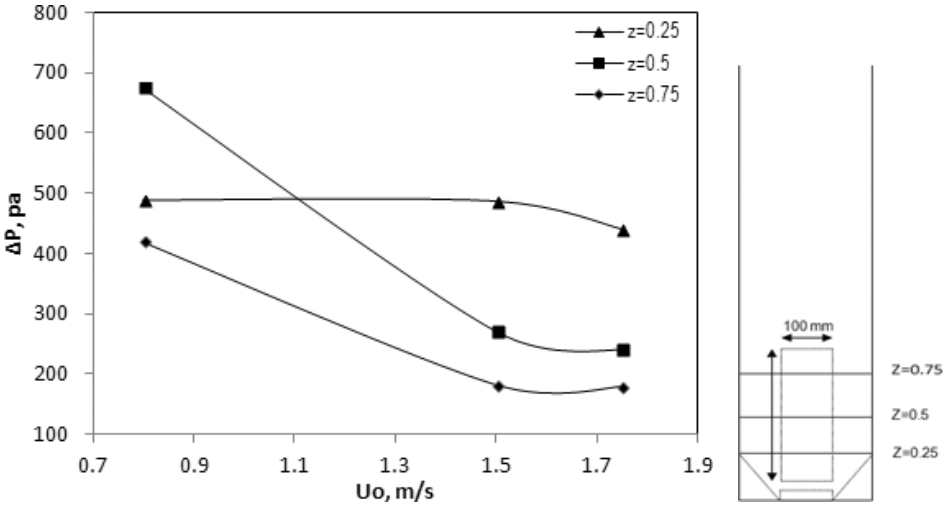

(a) (b)

Fig. 6. Pressure drop versus draft tube veolcity for the silica particle size $d_p = 86\,\mu$m.

4.3.2. *Solid circulation rate* (G_s)

Solid recirculation rate G_s is an important parameter to design any ICFB reactor with a suitable draft tube configuration. The effect of superfical gas velocity (Uo) on solid recirculation rate is shown in Fig. 7(a–c). Solids recirculation rate G_s is actually calculated based on the product of mean volume fraction of solids, density of solids and the solid velocity magnitude. G_s increases with Uo due to the increase in the driving force for the circulation of solids between the draft tube and downcomer and as a result an increased bed voidage is observed in the draft tube.

From Fig. 7(a), it can be observed that solids recirculation rate increases with draft tube inlet velocity up to the velocity of 1.5 m/s and then declained at higher

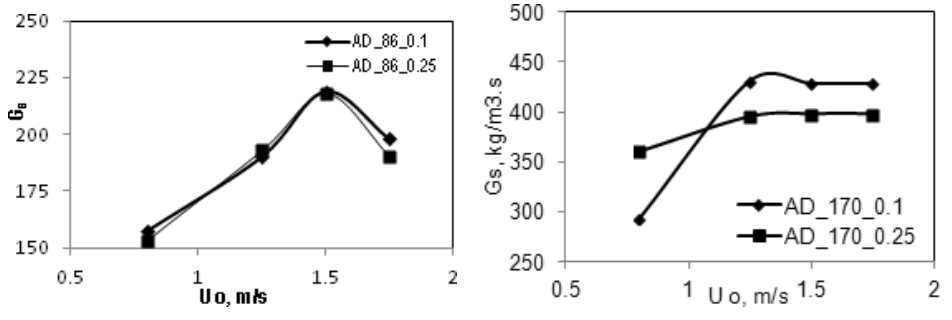

(a) (b)

Fig. 7. Solids circulation rate versus draft tube velocity: (a) 86 μm, (b) 170 μm and (c) 250 μm.

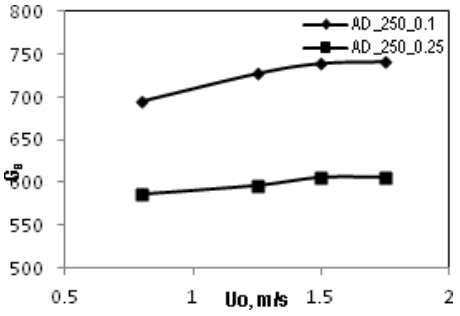

(c)

Fig. 7. (*Continued*)

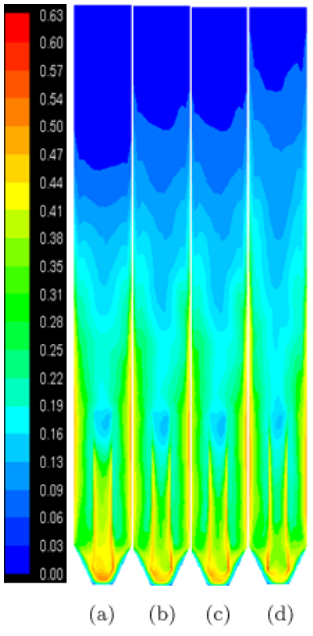

Fig. 8. Contour plot of solids volume fraction with different gas velocities of silica particles of size 86 μm at a constant annulus input velocity (with Arastoopour drag model) $U_a = 0.2$ m/s. (a) $U_d = 0.8$ m/s, (b) $U_d = 1.25$ m/s, (c) $U_d = 1.5$ m/s and (d) $U_d = 1.75$ m/s.

velocities. However, at higher superficial gas velocity, G_s decreases due to more air bypass from the draft tube to the annular region and also the rate of entrainment is more towards the annulus region. The air inlet velocity to the draft tube is maintained higher than the annulus inlet velocity, which makes the density difference between annular and draft tube to increase at higher velocity. This might be providing the driving force for the solids recirculation between the draft tube and the annular section. Further it is also observed in Figs. 7(a)–(c), that the solid curculation rate of smaller particles steeply increases with the increase of superficial

velocity than the coarser size particles. This is due to the resistance of small particles entering the draft tube through the gap opening is smaller than the large particles, thus more particles would enter the draft tube at the same velocities. And also less momentum is required for transport of the smaller particles in the draft tube to the annular bed column.

4.3.3. *Mean volume fraction countor plots*

Using the Arastoopour drag-based CFD model, predicted contours of solid phase volume fractions are shown in Figs. 8–10 for 86, 170 and 250 μm size silica particles at gas superficial velocities at 0.8, 1.25, 1.5 and 1.75 m/s, respectively. The bed expansion height for different size particles is clearly distinguished from these contour plots. Figure 8 displays the simulation results for particle size of 86 μm. It is found that the bed expansion is minimum at low superficial gas velocities. There exist a dense phase zone in the lower part of the ICFB and a dilute phase zone in the upper zone. However, the dense phase bed level decreases gradually with increasing superficial gas velocity from 0.8 to 1.75 m/s. As shown in Figs. 8(a)–(d), the solid distribution in the draft tube is significantly nonuniform. In case of 250 μm size particles as expected, the height of the bed expansion is lower compared to 170 and

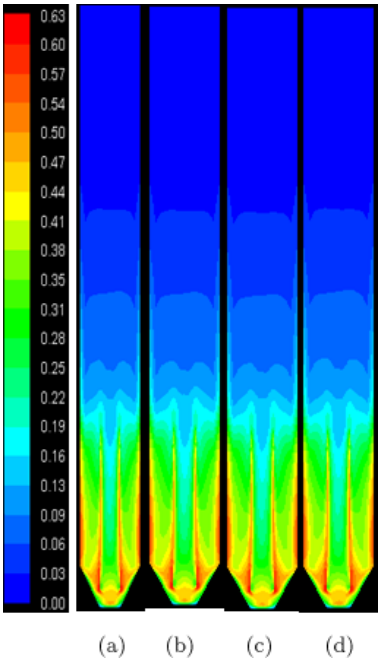

Fig. 9. Contour plot of mean solids volume fraction with different gas velocities of silica particles size 170 μm at constant annulus input velocity $U_a = 0.2$ m/s (with Arastoopour drag model). (a) $U_d = 0.8$ m/s, (b) $U_d = 1.25$ m/s, (c) $U_d = 1.5$ m/s and (d) $U_d = 1.75$ m/s.

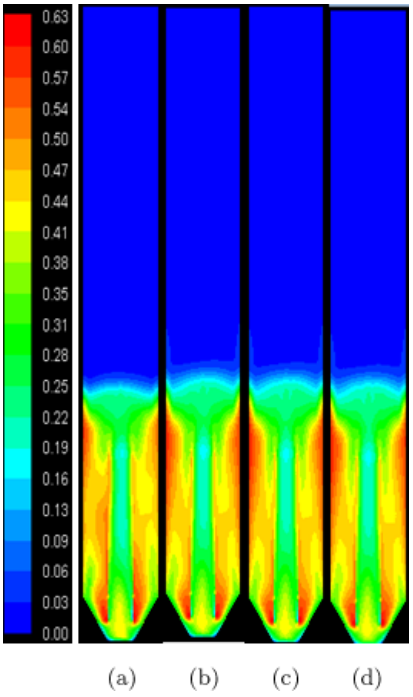

Fig. 10. Contour plot of mean solids volume fraction with different gas velocities of silica particles size 250 μm at constant annulus input velocity $U_a = 0.2$ m/s (with Arastoopour drag model). (a) $U_d = 0.8$ m/s, (b) $U_d = 1.25$ m/s, (c) $U_d = 1.5$ m/s and (d) $U_d = 1.75$ m/s.

86 μm particle profiles due to the increased effective weight of the coarse particles. The bed density in the bottom down corner has increased from average values of 0.28 to 0.45 solids volume fraction levels for 86 to 250 μm sized particles respectively. From Figs. 9 and 10 it is observed that the dynamics of bed are significantly effected by particle size and gas superficial gas velocities.

4.4. *Granular temperature profiles*

The granular temperature concept was first introduced into the literature by Lun *et al.* [1984]. The granular temperature is computed by solving a fluctuating kinetic energy equation for the particles as already discussed in the KTGF model in Sec. 2. The solid viscosity and granular pressure are computed as a function of granular temperature (Θ) in the CFD model itself, which are two kinds of turbulence in fluidization [Gidaspow *et al.* (2004)]. These two kinds of turbulence give to two kinds of mixing: one at the level of particles and other mixing at the level of bubbles or clusters. The classical or laminar granular temperature (Θ) is due to random oscillations of individual particles and turbulent granular temperature (Θ_t) is caused by the motion of clusters of particles or bubbles. The turbulent granular temperature is defined as the average of the normal Reynolds stresses [Jung and Gamwo (2005)]

which is the average of the three squares of the velocity components in the three directions by using the following definition.

$$\Theta_t = \frac{1}{3}\overline{v'_x v'_x} + \frac{1}{3}\overline{v'_y v'_y} + \frac{1}{3}\overline{v'_z v'_z}. \tag{31}$$

Total granular temperature is the sum of laminar granular temperature (Θ) equation (32) and turbulent granular temperature

$$\Theta_{\text{total}} = \Theta + \Theta_t. \tag{32}$$

4.4.1. *Particles granular temperatures*

Total granular temperature computed according to Eq. (32) for different superficial velocities and particle sizes. The bigger sized particles gave a low granular temperature due to the lower particle velocity fluctuations. At the wall, the granular temperature decreases, because of the wall frictional resistance for the particles. At the center of draft tube riser, the solid–solid interactions due to solid collisions were also low because of the low solid volume fraction. In the above draft tube section of the ICFB, the solid volume fraction decreases and causes the solid collisions to dominate the system.

Figure 11 shows the predicted solids granular temperature at superficial gas velocity of 1.25 m/s for different size range of solid particles (86, 170 and 250 μm). The predicted results indicate that the smaller solid particles have a high fluctuating velocity. The bigger size solid particles have low granular temperature due to the small fluctuating velocities. The particle fluctuating energy per unit of mass increased from the center of the draft tube towards the walls. At the wall, the granular temperature shows lower values because of the wall frictional effects. At the

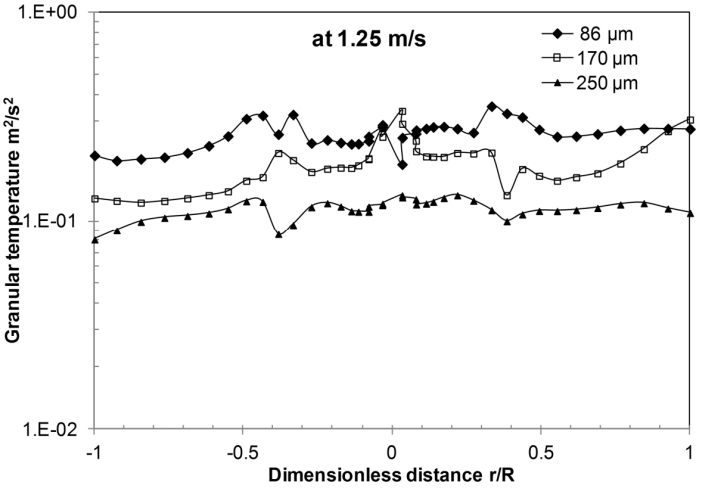

Fig. 11. Granular temperature profiles for 86, 170 and 250 μm particles at a velocity 1.25 m/s.

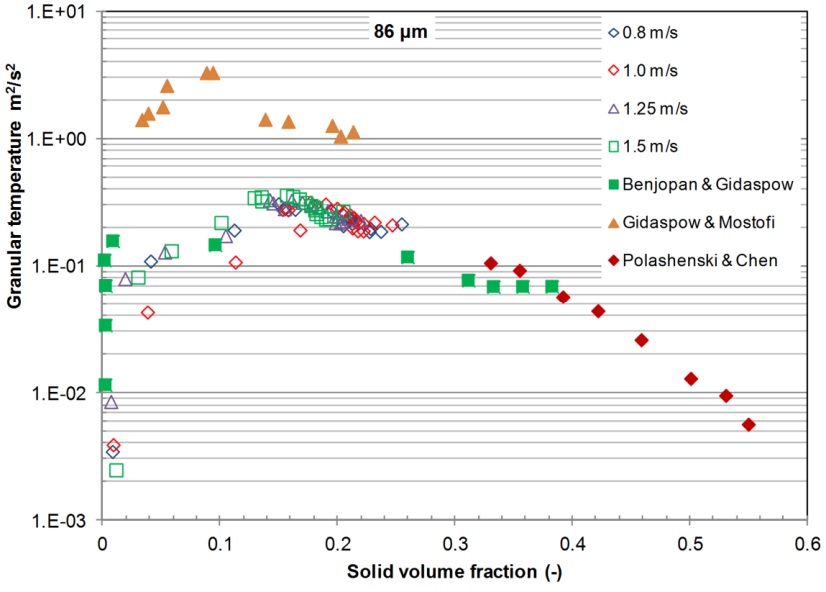

Fig. 12. Comparison of the theoretical granular temperatures derived in this study and those experimentally derived in the literature.

center of the draft tube, the particle–particle interactions due to particle collisions were also low because of low solid volume fraction.

Comparison of the computed total granular temperatures with literature-based experimental data for CFB [Chalermsinsuwana *et al.* (2011), Gidaspow and Mostofi (2003), Polashenski and Chen (1999)] is shown in Fig. 12. It is interesting to observe the variations of predicted granular temperature at different superficial velocities in the draft tube riser. A reasonable correct trend is shown between the predicted total granular temperature and the experimental data obtained by Benjopan *et al.* [2011]. There is a good agreement between the simulation results of 3D ICFB computational domains and with the experimental results from the literature at low solid volume fractions too. The total granular temperature tends to increase with increasing solids concentrations ($\varepsilon < 0.1$) in the dilute region and decreases with an increase of solids concentration in the dense region ($\varepsilon > 0.1$). In the dense zone, the decrease in the granular temperature is mainly due to the reduction of the mean free path of the solid particles. As the zone becomes that of the packed bed (high solids concentration), the granular temperature becomes very lean. Our predicted trends and magnitude of the total granular temperature agree with experimental data.

5. Conclusion

The hydrodynamic characteristic of 2D and 3D ICFB reactors gas–solid flow was studied by an Eulerian–Eulerian CFD model with the stress closer from KTGF. Four different drag models were considered for the simulations. Syamlal and

O'Brien, Gidaspow, Arastoopour and Gibilaro drag models are implemented into Fluent through the user defined functions (UDF). 2D simulation of an ICFB with polypropylene particles was run based on Ahuja and Patwardhan [2008] experimental case. Grid independence check is made with four grid sizes. The resulting hydrodynamic properties from 2D simulations are compared to Ahuja and Patwardhan [2008] experimental data. The simulation results by four different drag models show that the Arastoopour [1990] and Gibilaro drag models [1985] can accurately predict the flow pattern, voidage profiles and velocity profiles in the ICFB. With the Arastoopour drag model the simulations are giving the best fits to the experimental data. Further the CFD strategies on large scale for 3D ICFB, the comprehensive simulations data analysis is made with respect to scale-up design. The draft tube superficial gas velocity and the solids circulation rate have significant effect distribution of the solid volume fraction in each region. Increasing the draft tube superficial gas velocity can decreases solids volume fraction in the draft tube but has little effect in the annulus zone. The total granular temperature (Θ total) tends to increase with increasing solids concentrations ($\varepsilon < 0.1$) in the dilute region and decreases with an increase of solids concentration in the dense region ($\varepsilon > 0.1$). In the dense zone, the decreasing trend in the granular temperature is mainly due to the reduction of the mean free path of the solid particles.

Acknowledgment

The authors gratefully acknowledge funding support from the Ministry of Human Resource Department (MHRD) by Government of India.

References

Abu-Zaid, S. and Ahmadi, G. [1990] "A simple kinetic model for rapid granular flows including frictional losses," *ASCE J. Eng. Mech.* **116**, 379–389.

Ahuja, G. N. and Patwardhan, A. W. [2008] "CFD and experimental studies of solids hold-up distribution and circulation patterns in gas–solid fluidized beds," *Chem. Eng. J.* **143**, 147–160.

Arastoopour, H., Pakdel, P. and Adewumi, M. [1990] "Hydrodynamic analysis of dilute gas–solids flow in a vertical pipe," *Powder Technol.* **62**, 163–170.

Beetstra, R., van der Hoef, M. A. and Kuipers, J. A. M. [2007] "Numerical study of segregation using a new drag force correlation for polydisperse systems derived from lattice-Boltzmann simulations," *Chem. Eng. Sci.* **62**, 246–255.

Benjapon, C., Gidaspow, D. and Piumsomboona, P. [2011] "Two- and three-dimensional CFD modeling of Geldart A particles in a thin bubbling fluidized bed: Comparison of turbulence and dispersion coefficient," *Chem. Eng. J.* **171**, 301–313.

Benyahia, S., Arastoopour, H., Knowlton, T. and Massah, H. [2000] "Simulation of particles and gas flow behavior in the riser section of a circulating fluidized bed using the kinetic theory approach for the particulate phase," *Powder Technol.* **112**, 24–33.

Burugupalli, V. R. [1988] "Process analysis of a twin fluidized bed biomass gasification system," *Ind. Eng. Chem. Res.* **27**, 304–312.

Chalermsinsuwana, B., Gidaspow, D. and Pornpote Piumsomboona, B. [2011] "Two- and three-dimensional CFD modeling of Geldart A particles in a thin bubbling fluidized

bed: Comparison of turbulence and dispersion coefficient," *Chem. Eng. J.* **171**, 301–313.

Chan, C. K., Guo, Y. C. and Lau, K. S. [2005] "Numerical modeling of gas-particle flow using a comprehensive kinetic theory with turbulence modulation," *Powder Technol.* **150**, 42–55.

Chatterjee, A. [1970] "Effect of particle diameter and apparent particle density on internally solid circulation rate in air-spouted beds," *Ind. Eng. Chem. Res.* **9**, 531.

Feng, Y., Smith, T., Witt., P. J., Doblin, C., Lim, S. and Phil Schwarz, M. [2012] "CFD modeling of gas–solid flow in an internally circulating fluidized bed," *Powder Technol.* **219**, 78–85.

Gibilaro, L. G., Di Felice, R. and Foscolo, P. U. [1990] "Added mass effects in fluidized beds: application of the Geurst–Wallis analysis of inertial coupling in two-phase flow," *Chem. Eng. Sci.* **45**, 1561–1565.

Gibilaro, L. G., Di Felice, R. and Waldram, S. P. [1985] "Generalized friction factor and drag coefficient correlations for fluid–particle interactions," *Chem. Eng. Sci.* **40**, 1817–1823.

Gidaspow, D. [1994] "*Multiphase Flow and Fluidizationdization Continuum and Kinetic Theory Description* (Academic Press, New York).

Gidaspow, D., Jonghwun, J. and Singh, R. K. [2004] "Hydrodynamics of fluidization using kinetic theory: An emerging paradigm-2002 Flour–Daniel lecture," *Powder Technol.* **148**, 123–141.

Gidaspow, D. and Mostofi, R. [2003] "Maximum carrying capacity and granular temperature of A, B, and C particles," *AIChE J.* **49**, 831–843.

Helland, E., Bournot, H., Occelli, R. and Tadrist, L. [2007] "Drag reduction and cluster formation in a circulating fluidised bed," *Chem. Eng. Sci.* **62**, 148–158.

Hosseini, S., Ahmadi, G., Rahimi, R., Zivdarn M. and Esfahany M. [2010] "CFD studies of solids hold-up distribution and circulation patterns in gas–solid fluidized beds," *Powder Technol.* **200**, 202–215.

Hosseini, S. H., Zivdar, M., Rahimi, R. and Samimi, A. [2009] "CFD simulation of gas-solid bubbling fluidized bed containng the FCC particles," *Korean J. Chem. Eng.* **26**, 1405–1413.

Huilin, L., Yurong, H., Wentie, L., Jianmin, D., Gidaspow, D. and Bouillard, J. [2004] "Computer simulations of gas–solid flow in spouted beds using kinetic-frictional stress model of granular flow," *Chem. Eng. Sci.* **59**, 865–878.

Jeon, J. H. and Kim, S. D. [2010] "Hydrodynamic characteristics of binary solids mixtures in a square internally circulating fluidized bed," *J. Chem. Eng. Japan* **43**, 26–131.

Johnson, P. C. and Jackson, R. [1987] "Frictional-collisional constitutive relations for granular materials with application to plane shearing," *J. Fluid. Mech.* **176**, 67–93.

Jung, J., Gidspoan, D. and Gamwo, I. K. [2005] "Measurement of two kinds of granular temperatures, stresses and dispersion in bubbling beds," *Ind. Eng. Chem. Res.* **44**, 1329–1341.

Kim, S. D., Kim, Y. H., Roh, S. H. and Lee, D. H. [2002] "Solid circulation characteristics in an internally circulating fluidized bed with orifice-type draft tube," *Korean J. Chem. Eng.* **19**, 911.

Kim, Y. J., Lee, J. M. and Kim, S. D. [1997] "Coal gasification characteristics in an internally circulating fluidized bed with draught tube," *Fuel*, 1067.

Kim, Y. J., Lee, J. M. and Kim, S. D. [2000] "Modeling of coal gasification in an internally circulating fluidized bed reactor with draught tube," *Fuel* **79**, 69.

Kim, Y. T., Song, B. H. and Kim, S. D. [1997] "Entrainment of solids in an internally circulating fluidized bed with draft tube," *Chem. Eng. J.* **66**, 105–110.

Lun, C. K. K., Savage, S. B., Jeffrey, D. J. and Chepurniy, N. [1984] "Kinetic theories for granular flow: Inelastic particles in Couette flow and slightly inelastic particles in a general flow field," *J. Fluid Mech.* **140**, 223–256.

Marschall, K. J. and Mleczko, L. [1999] "CFD modeling of an internally circulating fluidized-bed reactor," *Chem. Eng. Sci.* **54**, 2085–2093.

McKeen, T. and Pugsley, T. [2003] "Simulation and experimental validation of a freely bubbling bed of FCC catalyst," *Powder Technol.* **129**, 139–152.

Milne, B., Berruti, F., Behie, L. A. and Brujin, T. J. W. [1992] "The internally circulating fluidized bed [ICFB]: A novel solution to gas bypassing in spouted beds," *Can. J. Chem. Eng.* **70**, 910.

Mujumdar, A. S. and Wu, Z. [2008] "Thermal drying technologies — Cost-effective innovation aided by mathematical modeling approach," *Drying Technol.* **26**, 146–154.

Neri, A. and Gidaspow, D. [2000] "Riser hydrodynamics: Simulation using kinetic theory," *AIChE J.* **46**, 52–67.

Passalacqua, A. and Marmo, L. [2009] "A critical comparison of frictional stress models applied to the simulation of bubbling fluidized beds," *Chem. Eng. Sci.* **64**(12), 2795–2806.

Patankar, S. V. [1980] *Numerical Heat Transfer and Fluid Flow* (Hemisphere Publishing Corporation, Washington).

Patil, D. J. and van Sint Annaland, M. [2005] "Critical comparison of hydrodynamic models for gas–solid fluidized beds—Part II: Freely bubbling gas–solid fluidized beds," *Chem. Eng. Sci.* **60**, 73–84.

Patil, D. J., van Sint Annaland, M. and Kuipers, J. A. M. [2005] "Critical comparison of hydrodynamics models for gas–solid fluidized beds—Part I: Bubbling gas–solid fluidized beds operated with a jet," *Chem. Eng. Sci.* **60**, 57–72.

Polashenski, W. and Chen, J. [1999] "Measurement of particle stresses in fast fluidized beds," *Ind. Eng. Chem. Res.* **38**, 705–713.

Reuge, N., Cadoret, L., Coufort-Saudejaud, C., Pannala, S., Syamlal, M. and Caussat, B. [2008] "Multi-fluid Eulerian modeling of dense gas–solid fluidized bed hydrodynamics; influence of the dissipation parameters," *Chem. Eng. Sci.* **22**, 5540–5551.

Schaeffer, D. G. [1987] "Instability in the evolution equations describing incompressible granular flow," *J. Differ. Equat.* **66**, 19–50.

Shirvanian, P. A. and Calo, J. M. [2004] "Hydrodynamic scaling of a rectangular spouted vessel with a draft duct," *Chem. Eng. J.* **103**, 29–34.

Shuyan, W., Xiang, L., Huilin, L., Long, Y., Dan, S., Yurong, H. and Yonglong, D. [2009] "Numerical simulations of flow behavior of gas and particles in spouted beds using frictional kinetic stresses model," *Powder Technol.* **196**, 184–193.

Sinclair, J. L. and Jackson, R. [1989] "Gas-particle flow in a vertical pipe with particle–particle interactions," *AIChE J.* **35**, 1473–1486.

Srivastava, A. and Sundaresan, S. [2003] "Analysis of a frictional-kinetic model for gas-particle flow," *Powder Technol*, **129**, 72–85.

Syamlal, M. and O'Brien, T. J. [1989] "Computer simulation of bubbles in a fluidized bed," *AIChE Symp. Ser.* **85**, 22–31.

Syamlal, M., Rogers, W. and O'Brien, T. J. [1993] "MFIX documentation: Theory guide." Technical note, Morgantown Energy Technology Centre, Morgantown, West Virginia.

Szafran, R. G. and Kmiec, A. [2007] "Periodic fluctuations of flow and porosity in spouted beds," *Transp. Porous Media* **66**, 187–200.

VanWachem, B. G. M., Schouten, J. C., van den Bleek, C. M., Krishna, R. and Sinclair, J. L. [2001] "Comparative analysis of CFD models of dense gas–solid systems," *AIChE J.* **47**, 1035–1051.

Wen, C. Y. and Yu, Y. H. [1966] "Mechanics of fluidization," *Chem. Eng. Prog. Symp. Ser.* **62**, 100–111.

Yang, N., Wang, W., Ge, W. and Li, J. [2003] "CFD simulation of concurrent-up gas–solid flow in circulating fluidized beds with structure-dependent drag coefficient," *Chem. Eng. J.* **96**, 71–80.

Yang, T., Zhang, T. and Bi, H. T. [2008] "A novel continuous reactor for catalytic reduction of NO_x — Fixed bed simulation," *Can. J. Chem. Eng.* **86**(3), 395–402.

Yang, W. C. and Keairns, D. L. [1978] "Design of recirculating fluidized beds for commercial applications," *AIChE Symp. Ser.* **74**, 218–228.

Zhao, X. L., Li, S. Q., Liu, G. Q., Song, Q. and Yao, Q. [2008] "Flow patterns of solids in a two-dimensional spouted bed with draft plates: PIV measurement and DEM simulations," *Powder Technol.* **183**, 79–87.

Zheng, Y., Wan, X., Qian, Z., Wei, F. and Jin, Y. [2001] "Numerical simulation of the gas–particle turbulent flow in riser reactor based on k–ε–kp–_p–two-fluid model," *Chem. Eng. Sci.* **56**, 6813–6822.

Zimmermann, S. and Taghipour, F. [2005] "CFD modeling of the hydrodynamics and reaction kinetics of FCC fluidized-bed reactors," *Ind. Eng. Chem. Res.* **44**, 9818–9827.